DOE/ER/10814-15



# INTERDIFFUSION IN THE Ni-Cr-Co-Mo SYSTEM AT 1300°C

by

J. A. Heaney, III and M. A. Dayananda*

DOE/ER/10814--15

DE86 011453

## ABSTRACT

Interdiffusion was investigated with solid-solid diffusion couples in the $\alpha$ (fcc) region of the quaternary Ni-Cr-Co-Mo system at 1300°C for the determination of diffusion paths and diffusional interactions among the components. The concentration profiles for a given couple exhibited a common cross-over composition, $\mathbf{Y}_c$, which reflected the relative depths of diffusion in the terminal alloys. Interdiffusion fluxes were calculated directly from the concentration profiles and the quaternary interdiffusion coefficients were calculated at selected compositions. Ni and Co exhibited up-hill diffusion against their individual concentration gradients in a direction opposite to the interdiffusion of Cr. Quaternary diffusion paths were presented as a set of partial diffusion paths on the basis of relative concentration variables.



## DISCLAIMER



*J. A. Heaney, III is with the Aircraft Engine Business Group, General Electric Company, Cincinnati, OH 45215-6301 and M. A. Dayananda is Professor of Materials Engineering, Purdue University, W. Lafayette, IN 47907.

## DISCLAIMER

# INTRODUCTION

In metallurgical systems, especially in high temperature applications, diffusion is of extreme importance, as it affects the kinetics and mechanisms of phase transformations, the stability of structures, and the oxidation-corrosion behavior of alloys. Most practical alloys are composed of more than two components and the "superalloys" may have as many as 10 or more components. The diffusion behavior in multicomponent alloys is more complicated than that in binary alloys where there exists only one independent concentration variable. In multicomponent systems the interactions among the components affect the interdiffusion process. These interactions may take the form of diffusion of a component up its own concentration gradient or the development of zero-flux planes and flux reversals [1-5] for the individual components. The understanding of these phenomena is of practical importance, since it involves the preferential distribution of a component in an alloy which may affect the integrity of the alloy.

Isothermal ternary diffusion studies have been carried out in several high temperature alloy systems, such as Fe-Ni-Co [6], Fe-Ni-Al [7], Co-Ni-Cr [8] and Fe-Ni-Cr [9] for the determination of interdiffusion coefficients and diffusion paths. Systematic interdiffusion studies in alloys with more than three components are limited in the literature and studies of quaternary diffusion have been recently reported in the Cu-Ni-Zn-Mn system [10,5].

The main objective of this study was to investigate interdiffusion with $\alpha$ (fcc) Ni-Cr-Co-Mo quaternary alloys at 1300°C with solid-solid diffusion couples and to determine quaternary diffusion paths. The samples were assembled with alloys characterized by similar concentrations for one or two of the components. The concentration profiles and diffusion paths were examined on the basis of relative

concentration variables and diffusion path parameters [2,5,10], and the paths were presented as a set of two partial diffusion paths. Quaternary interdiffusion coefficients were also calculated at selected compositions including those of maxima, minima and zero-flux planes (ZFP) in concentration profiles.

The Ni-Cr-Co-Mo system was chosen since it forms the basis of many high temperature and corrosion resistant alloys [11]. The fcc solid solution region is appreciable at 1200°C for Mo concentrations up to 20 wt.% [12]. Also, interdiffusion studies have been carried out in the binary Ni-Cr [13-16], Ni-Co [16-18], Ni-Mo [16,19,20], Co-Cr [16,21,22], and Co-Mo [16,19] systems and the ternary Co-Ni-Cr system [8].

## EXPERIMENTAL PROCEDURE

The compositions for the Ni-Cr-Co-Mo alloys employed in this study were selected to cover the concentration ranges normally encountered in high temperature applications. The concentration ranges are 0-25 wt.pct. for Co and Cr, and 0-10 wt.pct. for Mo. The alloys were prepared with Ni (99.9 pct), Cr (99.9 pct), Co (99.9 pct)) and Mo (99.97 pct) metals by induction melting in alumina crucibles in an argon atmosphere. The alloys were cast into rods by drawing the melts into 1 cm diameter quartz tubes. The alloy rods were swaged to about 30 percent reduction, sealed in quartz tubes which were evacuated and back-filled with argon to 350 $\mu$m of pressure. The alloys were homogenized at 1350°C for 4 days. The compositions of the various alloys analyzed by wet chemical techniques are presented in Table I.

The alloys were cut into disks about 5 mm in thickness with an Isomet diamond impregnated cut-off wheel. The parallel faces of the disks were metallographically polished through 0.05 $\mu$m alumina. Diffusion couples were assembled by clamping

together disks of selected alloys in a jig made of Kovar steel. The couples were encapsulated in quartz tubes evacuated and back-filled with argon to 350 $\mu$m pressure. The couples were diffusion annealed at 1300°C in a Lindberg heavy duty, three-zone tube furnace for 4 days with temperature controlled to $\pm$ 1°C. The annealed couples were quenched in ice-water. The couples were then cold mounted and sectioned parallel to the diffusion direction with an Isomet cut-off wheel. The sectioned couples were metallographically prepared and analyzed for concentration profiles by employing a point-to-point counting technique with a JELCO CF-35 scanning electron microscope equipped with an EDAX energy dispersive X-ray analyzer. X-ray spectra of Ni $K_\alpha$ (7.477 KeV), Cr $K_\alpha$ (5.414 KeV), Co $K_\alpha$ (6.930 KeV) and Mo $L_\alpha$ (2.293 KeV) were collected and stored on floppy disks. The spectra were analyzed for compositions with the aid of an EDAX 9100/60 system employing a ZAF correction program (NBS-Frame C) and pure element standards. For each couple, the composition profiles were determined by two independent traces. The data for the traces agreed within the uncertainty of $\pm$ 0.25 atom percent associated with the compositional analysis and were curve-fitted by a least squares cubic spline approximation.

## RESULTS

The quaternary Ni-Cr-Co-Mo diffusion couples employed in this study were assembled with terminal alloys of compositions presented in Table I and are listed in Table II. The couples are presented under three groups.

### A. Couples with Similar Terminal Concentrations for Two Components - Group I.

As indicated in Table II, the four couples in this group 6/7, 6/4, 4/7 and 5/10, were characterized by similar concentrations in the terminal alloys for two of the

components.

The couple 6/7 was characterized by similar terminal concentrations for Mo as well as for Ni. The concentration profiles for the couple are presented in Fig. 1. The concentration of each component i is expressed in atom percent as well as in relative concentration $Y_i$ defined by:

$$Y_i = \frac{C_i - C_i^+}{C_i^- - C_i^+} \qquad (i=1,2,3,4) \tag{1}$$

where $C_i^-$ and $C_i^+$ refer to the initial concentrations of component i in the terminal alloy disks of a couple. In Fig. 1 $x_o$ refers to the Matano plane.

The internal consistency among the profiles can be appreciated from the $Y_i$ vs x plots in Fig. 1(b). The plots cross one another at a common relative concentration $Y_c$ identified at the cross-over plane $x_c$. The profiles need to satisfy the consistency relation [2] given by:

$$\int_{L^-}^{x_c} (Y_j - Y_i)dx = \int_{x_c}^{L^+} (Y_i - Y_j)dx \qquad (i \neq j) \tag{2}$$

where the locations $L^-$ and $L^+$ are selected to cover the effective diffusion zone. Equation (2) implies that on either side of $x_c$ the area between the profiles of any two components i and j is the same. The matching of areas such as A and B between the Co and Ni profiles and of areas M and N between Cr and Co profiles on the two sides of $x_c$ is found to be within a difference of 10 percent. The large variation in the $Y_i$ values of Ni over the diffusion zone is due to the small difference in the Ni concentrations of the terminal alloys which yields a small denominator in Eq. (1). The maximum and minimum developed in the Ni concentration profile yield $Y_i$ values beyond the normal range, 0 to 1, expected for profiles with no maximum or minimum.

The interdiffusion flux $\tilde{J}_i$ of component i can be determined as a function of x directly from its concentration profile from the relation [1,2]:

$$\tilde{J}_i(x) = \frac{1}{2t}\left[\int_{C_i^+ \text{or} C_i^-}^{C_i(x)} (x-x_o)dC_i\right] \qquad (i=1,2,...,n) \tag{3}$$

where the variation in molar volume is considered negligible in the diffusion zone.

Profiles of interdiffusion fluxes for the couple 6/7 calculated on the basis of Eq. (3) are presented in Fig. 2(a). The interdiffusion flux of Cr is positive in the direction from alloy 6 to alloy 7, while the interdiffusion flux of Co is negative over the entire diffusion zone. The interdiffusion flux of Ni is from alloy 7 to alloy 6 and reflects up-hill diffusion against its own concentration gradient on the basis of the maximum and minimum developed in the Ni concentration profile shown in Fig. 1(a). The interdiffusion of Mo is considered negligible, since its profile is essentially flat in Fig. 1(a).

The sequence of compositions developed in the diffusion zone constitutes the diffusion path and for a quaternary diffusion couple the path can be presented as a space curve by plotting three independent concentration variables in three dimensions. Alternatively, the quaternary diffusion path can be presented as a set of two independent partial diffusion paths obtained by plotting the relative concentrations of two of the components against that of a third component. Such a set of partial diffusion paths obtained by plotting $Y_{Cr}$ and $Y_{Ni}$ against $Y_{Co}$ for the couple 6/7 is shown in Fig. 2(b). The paths are S-shaped and cross the straight line joining the terminal compositions at the cross-over composition $Y_c$, which is considered a characteristic parameter for the couple.

The concentration profiles and the diffusion path for the couple 6/4, characterized by similar terminal concentrations for both Cr and Mo, are presented in Fig. 3. As can be seen in Fig. 3(a) the concentration profile of Mo remained essentially flat while Ni and Co interdiffused in opposite directions. The Cr gradients and fluxes are quite small and as shown in Fig. 3(b) the diffusion path is represented by a plot of $Y_{Co}$ vs. $Y_{Ni}$.

The terminal alloys for the couple 4/7 had similar Co and Mo concentrations and the concentration profiles for the couple are presented in Fig. 4(a). The profiles of Mo and Co remain essentially flat indicating that the interdiffusion of Ni and Cr in opposite directions have negligible interactions on the interdiffusion of Co and Mo. The diffusion path for the couple is presented in Fig. 4(b) as a plot of $Y_{Ni}$ vs. $Y_{Cr}$ and it is essentially a straight line.

The couple 5/10 was characterized by similar terminal concentrations of Ni as well as of Cr and the concentration profiles and the diffusion path representation for the couple are presented in Fig. 5. The Cr profile remains virtually flat and the diffusion path is represented by a set of plots of $Y_{Ni}$ and $Y_{Co}$ vs. $Y_{Mo}$ exhibiting a common cross-over at the composition $Y_c$.

## B. Couples with Similar Terminal Concentrations for One Component - Group II

The diffusion couples 3/4 and 10/7 in this group were characterized by similar terminal concentrations of Mo and Co, respectively. For the couple 3/4 the initially flat profile of Mo remained unaffected by the interdiffusion of Ni, Co and Cr; this is similar to the flat Mo profile observed for the couple 6/4 in Fig. 3(a). The diffusion path for the couple 3/4 is presented in Fib. 6(a) as a set of partial paths of $Y_{Ni}$ and $Y_{Co}$ vs. $Y_{Cr}$ with a common cross-over composition at $Y_c$.

For the couple 10/7, the initially flat profile of Co was affected little by the interdiffusion of the other elements. This observation was similar to the flat Co profile observed for the couple 4/7 in Fig. 4(a). The diffusion path for the couple 10/7 is presented in Fig. 6(b) as plots of $Y_{Ni}$ and $Y_{Cr}$ vs. $Y_{Mo}$; since the two partial paths essentially coincide with each other, they are shown as a single curve.

## C. Couple With Dissimilar Terminal Concentrations - Group III

The couple 3/10 in this group was assembled with terminal alloys having dissimilar concentrations of each component. Concentration profiles for the couple 3/10 are presented in Fig. 7. The concentration profile for Co exhibits a relative maximum on the alloy 10 side of the diffusion zone, as can be seen in Fig. 7(a). The development of the maximum in the Co concentration profile reflects uphill diffusion of Co against its own concentration gradient. The concentration profiles expressed on the relative concentration variable basis are shown in Fig. 7(b). The profiles of Ni, Cr, Co and Mo cross at a common relative composition, $Y_c$, at the cross-over plane, $x_c$. The maximum developed in the Co concentration profile yields $Y_i$ values less than zero.

Profiles of the interdiffusion fluxes, calculated on the basis of Eq. (3), are presented in Fig. 8(a). The interdiffusion flux profile for Co indicates the development of a zero-flux plane (ZFP) in the diffusion zone and a reversal in its flux direction. To the left of the ZFP the interdiffusion flux for Co is negative from alloy 10 to alloy 3, while to the right of the ZFP the flux of Co is positive from alloy 3 to alloy 10. The interdiffusion fluxes of Mo and Ni are positive while the flux of Cr is negative.

The diffusion path for this couple is presented in Fig. 8(b) as a set of plots of $Y_{Co}$, $Y_{Cr}$, and $Y_{Ni}$ verses $Y_{Mo}$. Any two of these three partial paths would describe the diffusion path for the quaternary couple. The partial paths cross the straight line joining the terminal alloys at $Y_c$.

## DISCUSSION

The various single phase solid-solid quaternary diffusion couples investigated in this study indicated the existence of a common cross-over composition where the relative concentrations $Y_i$'s for all components are equal to $Y_c$. $Y_c$ can be identified not only from the concentration profiles as shown in Figs. 1(b) and 7(b) but also from the diffusion paths for the various couples in Figs. 2(b), 3(b), 5(b), 6 and 8(b). Values of $Y_c$ for the various couples are reported in Table III. The estimated uncertainty in these values is $\pm$ 0.02 on the relative concentration scale. These observations are similar to those reported for quaternary diffusion couples in the Cu-Ni-Zn-Mn system [10].

The cross-over composition $Y_c$ is considered a characteristic parameter for a given couple. One of the interpretations for $Y_c$ is that it represents the common average relative concentration for each component over the effective diffusion zone of the couple [2,5]. Thus, $Y_c$ is expressed by

$$Y_c = \frac{1}{(L^+ - L^-)} \int_{L^-}^{L^+} Y_i \, dx \qquad (i=1,2,...,n) \tag{4}$$

where $L^+$ and $L^-$ locations cover the diffusion zone for all n components and satisfy the relation:

$$\frac{Y_c}{1 - Y_c} = \frac{x_o - L^-}{L^+ - x_o} \tag{5}$$

Thus, the effective depths of diffusion on either side of the Matano plane, $x_o$, can be considered proportional to $Y_c$ and $1 - Y_c$. Values of the ratio $Y_c/(1-Y_c)$ and the ratio of the observed diffusion depths $(x_o-L^-)/(L^+-x_o)$ on the two sides of the Matano plane are also reported for the various couples in Table III. Within an uncertainty of ± 15 percent values of the ratio of the diffusion depths appear consistent with those of $Y_c/(1-Y_c)$.

The variation of the molar volume with composition is considered negligible for the couples in this study. On the basis of the lattice parameter data available for Ni-Cr [23], Co-Cr [23], Ni-Mo [24], Ni-Cr-Co [25] and Ni-Cr-Co-Mo [12] alloys, the molar volume variation for the alloys used in this investigation is considered to be within 5 percent of 7 cc/g·mole.

On the basis of Onsager's formalism [26] of Fick's law, the interdiffusion flux for a component in the Ni-Cr-Co-Mo quaternary system can be expressed by:

$$\tilde{J}_i = - \tilde{D}^{Ni}_{iCr} \frac{\partial C_{Cr}}{\partial x} - \tilde{D}^{Ni}_{iCo} \frac{\partial C_{Co}}{\partial x} - \tilde{D}^{Ni}_{iMo} \frac{\partial C_{Mo}}{\partial x} \quad (i=Cr,Co,Mo) \tag{6}$$

where Ni has been chosen as the dependent concentration variable. The experimental determination of the nine quaternary interdiffusion coefficients in Eq. (6) requires three independent diffusion couples with a common intersection of their diffusion paths and it is extremely hard to assemble such couples. From the individual quaternary diffusion couples in this study it is possible, however, to calculate some of the interdiffusion coefficients at selected compositions. For the couple 4/7, shown in Fig. 4, Co and Mo have negligible concentration gradients so that from Eq. [6] the interdiffusion flux of Cr is given by

$$\tilde{J}_{Cr} = - \tilde{D}^{Ni}_{CrCr} \frac{\partial C_{Cr}}{\partial x} \tag{7}$$

From the values of $\tilde{J}_{Cr}$ and $\partial C_{Cr}/\partial x$ calculated from the concentration profile for Cr for the couple 4/7, values for the main coefficient, $\tilde{D}^{Ni}_{CrCr}$ were determined at selected compositions. These values are presented in Table IV and plotted as a function of $N_{Cr}$ in Fig. 9(a). The interdiffusion coefficient, $\tilde{D}^{Ni}_{CrCr}$ increases with increasing Cr and exhibits a maximum at approximately 18 atm. pct. Cr. This observation is similar to the maximum in the binary interdiffusion coefficients reported for Ni-Cr binary alloys [15].

Another main coefficient $\tilde{D}^{Ni}_{CoCo}$ can also be calculated from the couple 4/6 where Mo and Cr have negligible concentration gradients, as shown in Fig. 3(a). Hence, for the flux of Co, Eq. (6) yields:

$$\tilde{J}_{Co} = - \tilde{D}^{Ni}_{CoCo} \frac{\partial C_{Co}}{\partial x} \tag{8}$$

From the values of $\tilde{J}_{Co}$ and $\partial C_{Co}/\partial x$ determined from the Co concentration profile, $\tilde{D}^{Ni}_{CoCo}$ was calculated at several compositions in the couple 4/6. These values are also presented in Table IV and plotted as a function of $N_{Co}$ in Fig. 9(b). The interdiffusion coefficient $\tilde{D}^{Ni}_{CoCo}$ decreases with increasing Co concentration similar to the observation reported for the binary interdiffusion coefficient for Ni-Co alloys [17]. The apparent minimum observed for $\tilde{D}^{Ni}_{CoCo}$ at approximately 15 atm pct. Co in Fig. 9(b) is similar to the minimum in the interdiffusion data reported for binary Ni-Co alloys by Kucera [18].

The maxima or minima that develop in the concentration profile of a component also aid in the calculation of selected interdiffusion coefficients. For the couple 6/7, in Fig. 1, the Ni concentration profile shows a maximum and a minimum where $\partial C_{Ni}/\partial x = 0$. At these locations $\tilde{J}_{Ni}$ can be expressed by

$$\tilde{J}_{Ni} = - \tilde{D}^{Co}_{NiCr} \frac{\partial C_{Cr}}{\partial x} \tag{9}$$

where Co is taken as the dependent component. Values for $\tilde{D}^{Co}_{NiCr}$ calculated at the maximum and minimum in the Ni profile are also included in Table IV.

At the maximum in the Co concentration profile for the couple 3/10 in Fig. 7(a), where $\partial C_{Co}/\partial x = 0$, the interdiffusion flux of Co from Eq. (6) is given by

$$\tilde{J}_{Co} = - \tilde{D}^{Ni}_{CoCr} \frac{\partial C_{Cr}}{\partial x} \tag{10}$$

where the concentration gradient for Mo is considered negligible. From the calculated values of $\tilde{J}_{Co}$ and $\partial C_{Cr}/\partial x$ at the Co maximum, a negative value for $\tilde{D}^{Ni}_{CoCr}$ was determined and is included in Table IV. Also, at the ZFP for Co observed in the couple 3/10, if the concentration gradient for Mo is considered negligible, the flux for Co is expressed by

$$\tilde{J}_{Co} = - \tilde{D}^{Ni}_{CoCo} \frac{\partial C_{Co}}{\partial x} - \tilde{D}^{Ni}_{CoCr} \frac{\partial C_{Cr}}{\partial x} = 0 \tag{11}$$

Hence,

$$\frac{\tilde{D}^{Ni}_{CoCr}}{\tilde{D}^{Ni}_{CoCo}} = - \left. \frac{\frac{\partial C_{Co}}{\partial x}}{\frac{\partial C_{Cr}}{\partial x}} \right|_{ZFP} \tag{12}$$

From the value of 1.7 for the ratio of the concentration gradients of Co and Cr at the ZFP and the value of $\tilde{D}^{Ni}_{CoCr}$ determined at the maximum in the Co concentration profile, a value for $\tilde{D}^{Ni}_{CoCo}$ was calculated and is also reported in Table IV.

Errors in the calculation of interdiffusion coefficients arise mainly from errors in the values of concentration gradients. The errors associated with the calculated interdiffusion coefficients in this study have been determined to be approximately $\pm$ 20 percent.

In the absence of quantitative thermodynamic data for the Ni-Cr-Co-Mo system, one may utilize the thermodynamic data available for the binary and ternary subsystems to gain a qualitative appreciation of the observed diffusional interactions. The activity of Ni shows negative deviations from ideality for $\alpha$ (fcc) Ni-Cr [27] and Ni-Co alloys [28], and Cr is more effective than Co in lowering the activity of Ni. This fact is consistent with the up-hill diffusion of Ni observed for the couple 6/7 in Fig. 1, where the concentration of Ni is similar in the terminal alloys. For the couple 6/7 the activity of Ni is expected to be lower on the alloy 6 side than on the side of alloy 7 and Ni can interdiffuse from alloy 7 into alloy 6 down its activity gradient. The interdiffusion of Ni against a concentration gradient of Cr in the couple 6/7 may also be appreciated from the calculated values for $\tilde{D}^{Co}_{NiCr}$ listed in Table IV. The negative values for $\tilde{D}^{Co}_{NiCr}$ indicate that the interdiffusion flux for Ni would be retarded down a Cr concentration gradient but enhanced against it. A negative value for the $\tilde{D}^{Ni}_{CoCr}$ coefficient at low Mo concentration also indicates that the interdiffusion flux of Co can be appreciably retarded down a Cr gradient but favored against it. These diffusional interactions of Cr gradients on the fluxes of Ni and Co are consistent with those observed for ternary Co-Ni-Cr alloys [8].

## ACKNOWLEDGMENTS

This research was supported by the Department of Energy under contract DE-AC02-81ER10814 and is based on a dissertation submitted by J. A. Heaney, III

to Purdue University in partial fulfillment of the requirements for the M.S. *degree in* Metallurgical Engineering.

## REFERENCES


1. M. A. Dayananda and C. W. Kim: Metall. Trans. A, 1979, vol. 10A, p. 1333.
2. M. A. Dayananda: Metall. Trans. A, 1983, vol. 14A, p. 1851.
3. C. W. Kim and M. A. Dayananda: Metall. Trans. A, 1983, vol. 14A, p. 857.
4. C. W. Kim and M. A. Dayananda: Metall. Trans. A, 1984, vol. 15A, p. 649.
5. M. A. Dayananda: Diffusion in Solids-Recent Developments, Edited by M. A. Dayananda and G. E. Murch, published by TMS-AIME, Warrendale, PA, 1985, p. 195.
6. J. P. Sabatier and A. Vignes: Mem. Sci. Rev. Metall., 1967, vol. 64, p. 225.
7. G. H. Cheng and M. A. Dayananda: Metall. Trans. A, 1979, vol. 10A, p. 1407.
8. A. G. Guy and V. Leroy: The Electron Microprobe, Edited by McKinley, Heinrich and Wittry, John Wiley and Sons, Inc., 1966 p. 543.
9. J. G. Duh and M. A. Dayananda: Diffusion and Defect Data, 1985, vol. 39, p. 1.
10. K. E. Kansky and M. A. Dayananda: Metall. Trans. A, 1985, vol. 16A, p. 1123.
11. C. T. Sims and W. C. Hagel: The Superalloys, John Wiley and Sons, Inc., New York, 1972, p. 197.
12. S. P. Rideout and P. Beck: NASA TR#1122, 1953.

13. A. Davin, V. Leroy, D. Counsouradis, and L. Habraken: Mem. Sci. Rev. Metall., 1963, vol. 60, p. 275.

14. T. Heumann and W. Reerink: Acta. Met., 1966, vol. 14, p. 201.

15. Y. E. Ugaste: Fiz. Met. Metalloved., 1967, vol. 24, p. 442.

16. A. Davin, V. Leroy, D. Coutsouradis, and L. Habraken: Cobalt, 1963, vol. 19, p. 51.

17. T. Ustad and H. Sorum: Phys. Stat. Solidi A, 1973, vol. 20, p. 285.

18. J. Kucera, K. Ciha and K. Stransky: Czech. J. Phys., 1977, vol. B27, p. 758.

19. C. P. Heijwegen and G. D. Rieck: Acta Met., 1974, vol. 22, p. 1269.

20. Y. E. Ugaste and N. V. Pimenov: Fiz. Metal. Metalloved. 1972, vol. 35, p. 125.

21. J. W. Weeton: Trans. ASM, 1952, vol. 44, p. 463.

22. A. Green, D. P. Whittle, J. Stringer and N. Swindells: Scripta Met., 1973, vol. 7, p. 1079.

23. N. Yukawa, Y. Fukano, M. Kawamura and T. Imura: Trans. Jap. Inst. Metals, 1968, vol. 9, p. 372.

24. R. E. W. Casselton and H. Hume-Rothery: J. Less Common Metals, 1964, vol. 7, p. 212.

25. W. O. Manly and P. A. Beck: NASA TR#2602, 1952.

26. L. Onsager: N. Y. Acad. of Sci., Annals, 1945-46, vol. 46, p. 241.

27. F. N. Mazandarany and R. D. Pehlke: Metall. Trans. A, 1973, vol. 4A, p. 2067.

28. J. Vrestal and J. Kucera: Metall. Trans. A, 1970, vol. 2A, p. 3367.

## FIGURE CAPTIONS

Fig. 1. Concentration profiles for the couple 6/7 with concentrations expressed in (a) atom percent and (b) relative concentrations, $Y_i$.

Fig. 2. (a) Profiles of interdiffusion fluxes and (b) the diffusion path representation for the couple 6/7.

Fig. 3. (a) Concentration profiles and (b) the diffusion path representation for the couple 6/4.

Fig. 4. (a) Concentration profiles and (b) the diffusion path for the couple 4/7.

Fig. 5. (a) Concentration profiles and (b) the diffusion path representation for the couple 5/10.

Fig. 6. Diffusion paths for (a) couple 3/4 and (b) couple 7/10.

Fig. 7. Concentration profiles for the couple 3/10 with concentrations in (a) atom percent and (b) relative concentrations.

Fig. 8. (a) Profiles of interdiffusion fluxes and (b) the diffusion path representation for the couple 3/10.

Fig. 9. Variation of quaternary interdiffusion coefficients (a) $\tilde{D}^{Ni}_{CrCr}$ and (b) $\tilde{D}^{Ni}_{CoCo}$ with composition, as calculated from the couples, 4/7 and 4/6, respectively.

TABLE I. Compositions of Ni-Cr-Co-Mo alloys.

| Alloy | Atomic Percent | | | |
|---|---|---|---|---|
| | Ni | Cr | Co | Mo |
| 3 | 82.1 | 11.7 | -- | 6.2 |
| 4 | 43.9 | 25.6 | 23.5 | 7.0 |
| 5 | 50.0 | 27.5 | 16.1 | 6.4 |
| 6 | 66.1 | 27.5 | -- | 6.2 |
| 7 | 65.0 | -- | 28.4 | 6.6 |
| 10 | 48.7 | 25.7 | 25.6 | -- |

TABLE II. Ni-Cr-Co-Mo solid-solid diffusion couples investigated at 1300°C.

| Group | Couple Designation | Similar Terminal Concentrations for |
|---|---|---|
| I | 6/7 | Mo and Ni |
| | 6/4 | Mo and Cr |
| | 4/7 | Mo and Co |
| | 5/10 | Ni and Cr |
| II | 3/4 | Mo |
| | 10/7 | Co |
| III | 3/10 | -- |

TABLE III. Experimental values of $Y_c/1-Y_c$ and the relative depths of diffusion in the terminal alloys for various diffusion couples.

| Couple | $Y_c$ | $\frac{Y_c}{1 - Y_c}$ | $\frac{x_o - L^-}{L^+ - x_o}$ |
|---|---|---|---|
| 6/7 | 0.67 | 2.0 | 1.8 |
| 6/4 | 0.51 | 1.0 | 1.0 |
| 5/10 | 0.57 | 1.3 | 1.1 |
| 3/4 | 0.45 | 0.82 | 1.0 |
| 10/7 | 0.41 | 0.7 | 1.0 |
| 3/10 | 0.51 | 1.0 | 1.2 |

TABLE IV. Calculated quaternary interdiffusion coefficients for Ni-Cr-Co-Mo alloys at 1300°C.

| Couple | Composition Atom % | | | | $\tilde{D}_{ij}^{Ni}\left(\frac{cm^2}{sec}\right)$ |
|---|---|---|---|---|---|
| | Ni | Cr | Co | Mo | X $10^{10}$ |
| 4/7 | | | | | $\tilde{D}_{CrCr}^{Ni}$ |
| | 44.3 | 24.2 | 24.1 | 7.4 | 7.5 |
| | 45.3 | 22.7 | 24.5 | 7.4 | 9.7 |
| | 46.8 | 20.8 | 25.0 | 7.4 | 9.9 |
| | 48.8 | 18.4 | 25.6 | 7.2 | 10.1 |
| | 51.6 | 15.2 | 25.8 | 7.4 | 8.2 |
| | 55.6 | 10.8 | 26.2 | 7.4 | 6.9 |
| | 58.8 | 6.4 | 27.1 | 7.7 | 6.4 |
| | 61.2 | 3.2 | 47.9 | 7.7 | 6.8 |
| 4/6 | | | | | $\tilde{D}_{CoCo}^{Ni}$ |
| | 64.9 | 26.8 | 1.7 | 6.6 | 8.9 |
| | 62.7 | 26.5 | 4.4 | 6.4 | 6.0 |
| | 59.7 | 26.3 | 7.4 | 6.6 | 4.8 |
| | 47.2 | 25.8 | 19.8 | 7.1 | 3.7 |
| | 45.7 | 25.8 | 21.4 | 7.1 | 4.2 |
| | 50.8 | 25.9 | 16.2 | 7.1 | 3.3 |
| 6/7 | | | | | $\tilde{D}_{NiCr}^{Co}$ |
| | 67.9 | 22.2 | 3.7 | 6.2 | -2.0 |
| | 62.0 | 6.5 | 23.9 | 7.6 | -1.7 |
| 3/10 | | | | | $\tilde{D}_{CoCr}^{Ni}$ |
| | 48.1 | 25.5 | 26.0 | 0.4 | -5.7 |
| | | | | | $\tilde{D}_{CoCo}^{Ni}$ |
| | 50.4 | 24.0 | 24.7 | 0.9 | 3.37 |

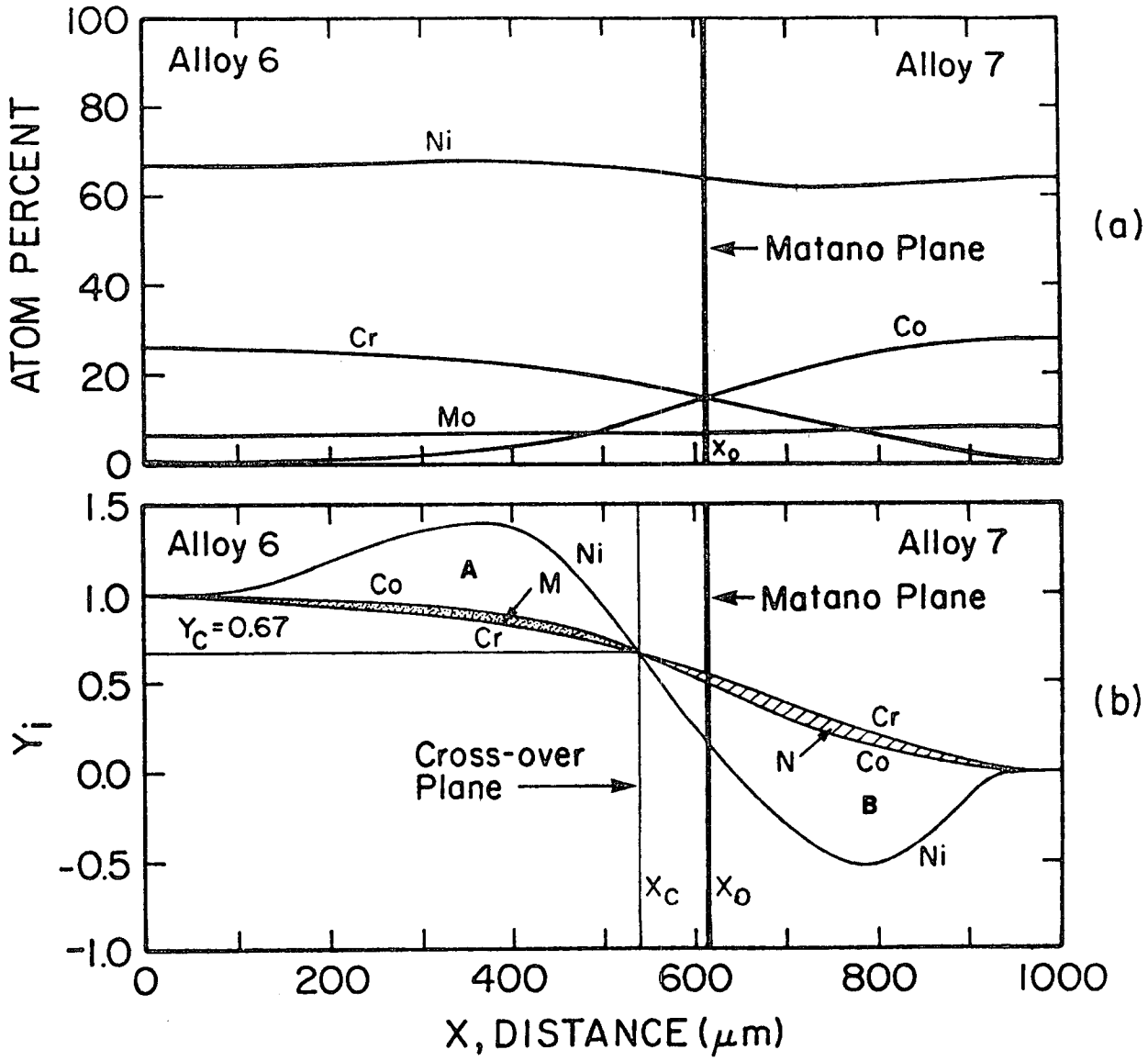


Fig. 1. Concentration profiles for the couple 6/7 with concentrations expressed in (a) atom percent and (b) relative concentrations, $Y_i$.

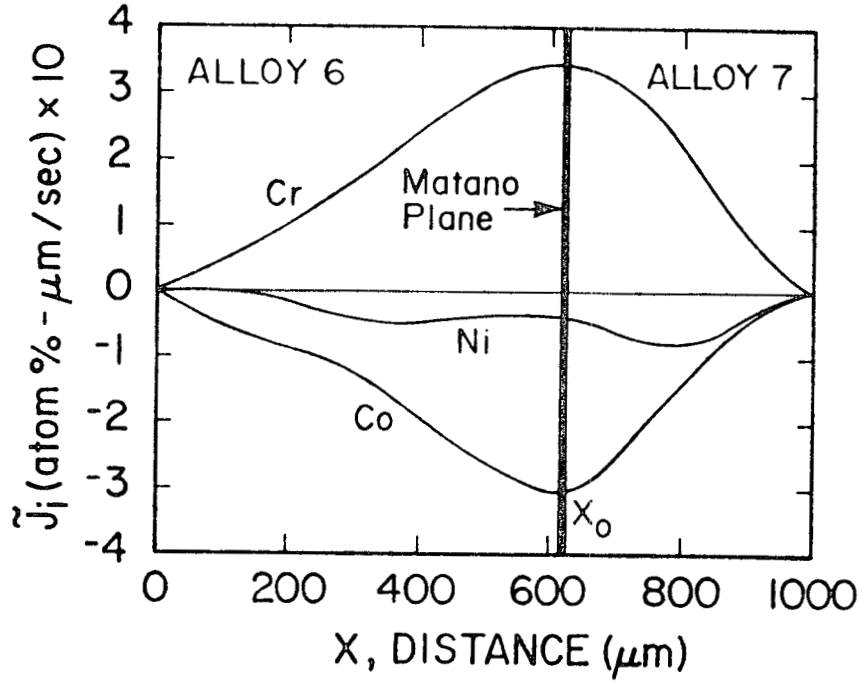


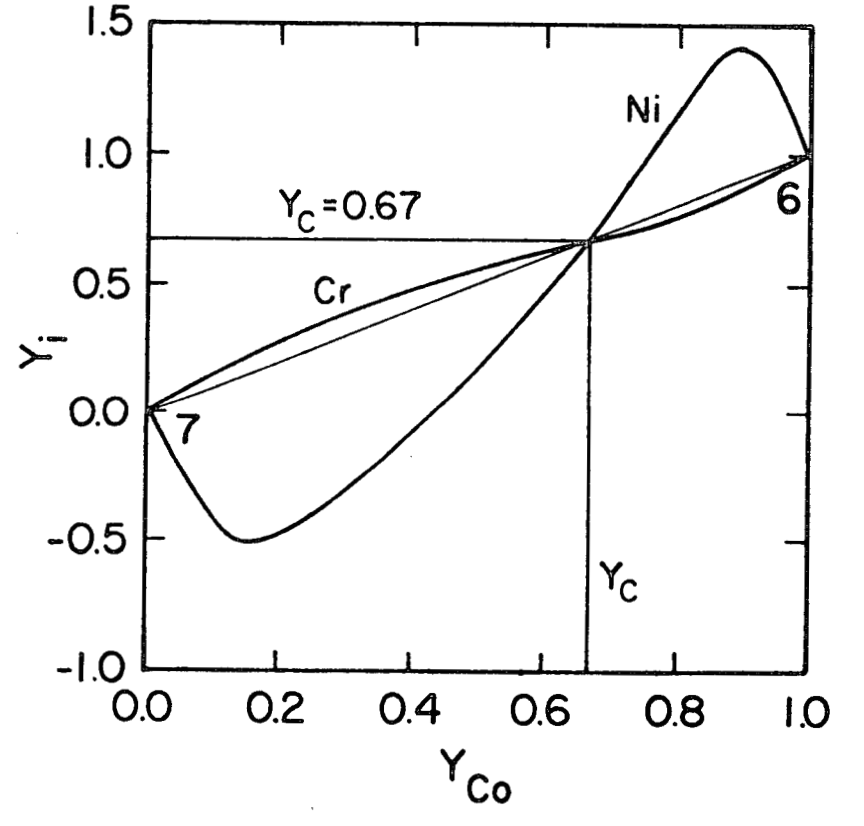


Fig. 2. (a) Profiles of interdiffusion fluxes and (b) the diffusion path representation for the couple 6/7.

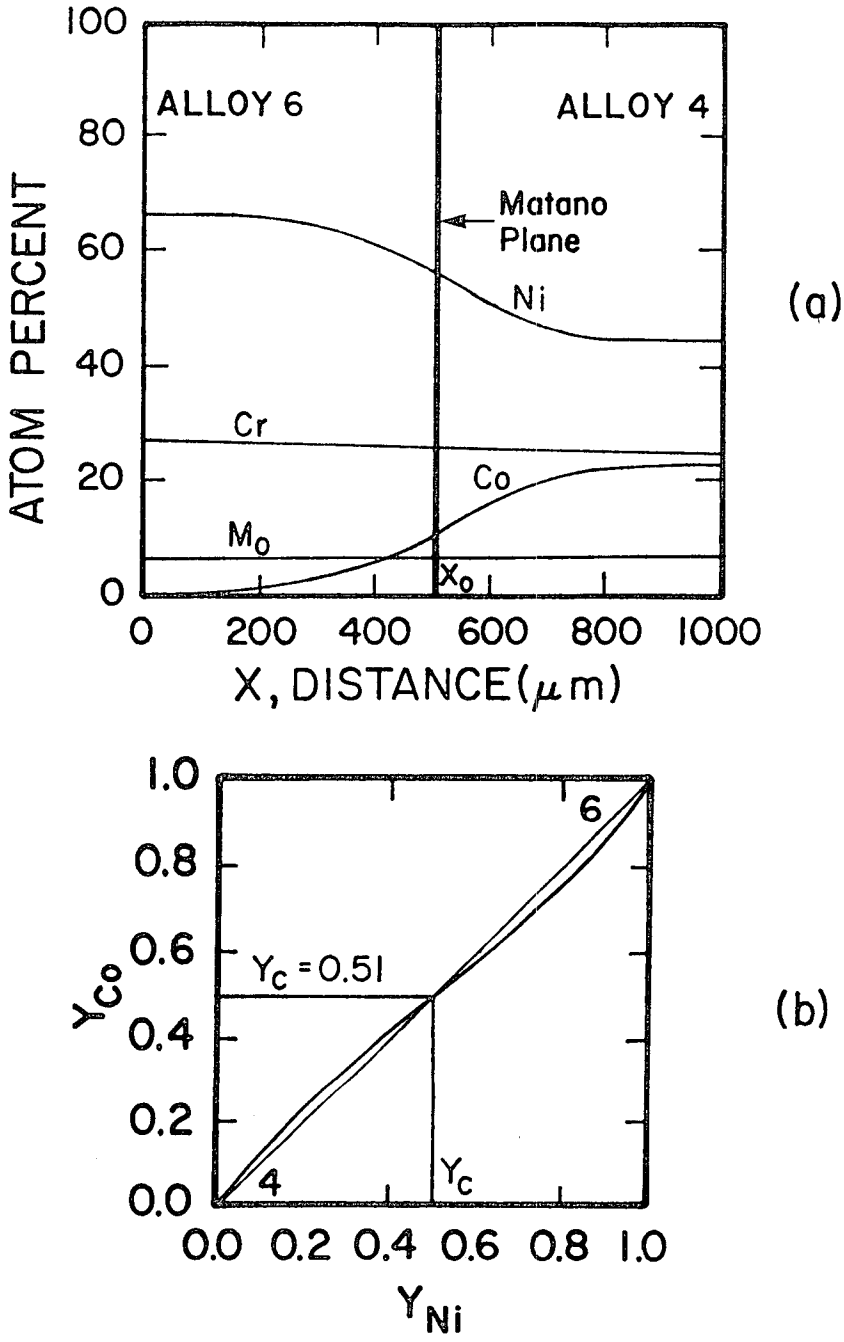


Fig. 3. (a) Concentration profiles and (b) the diffusion path representation for the couple 6/4.

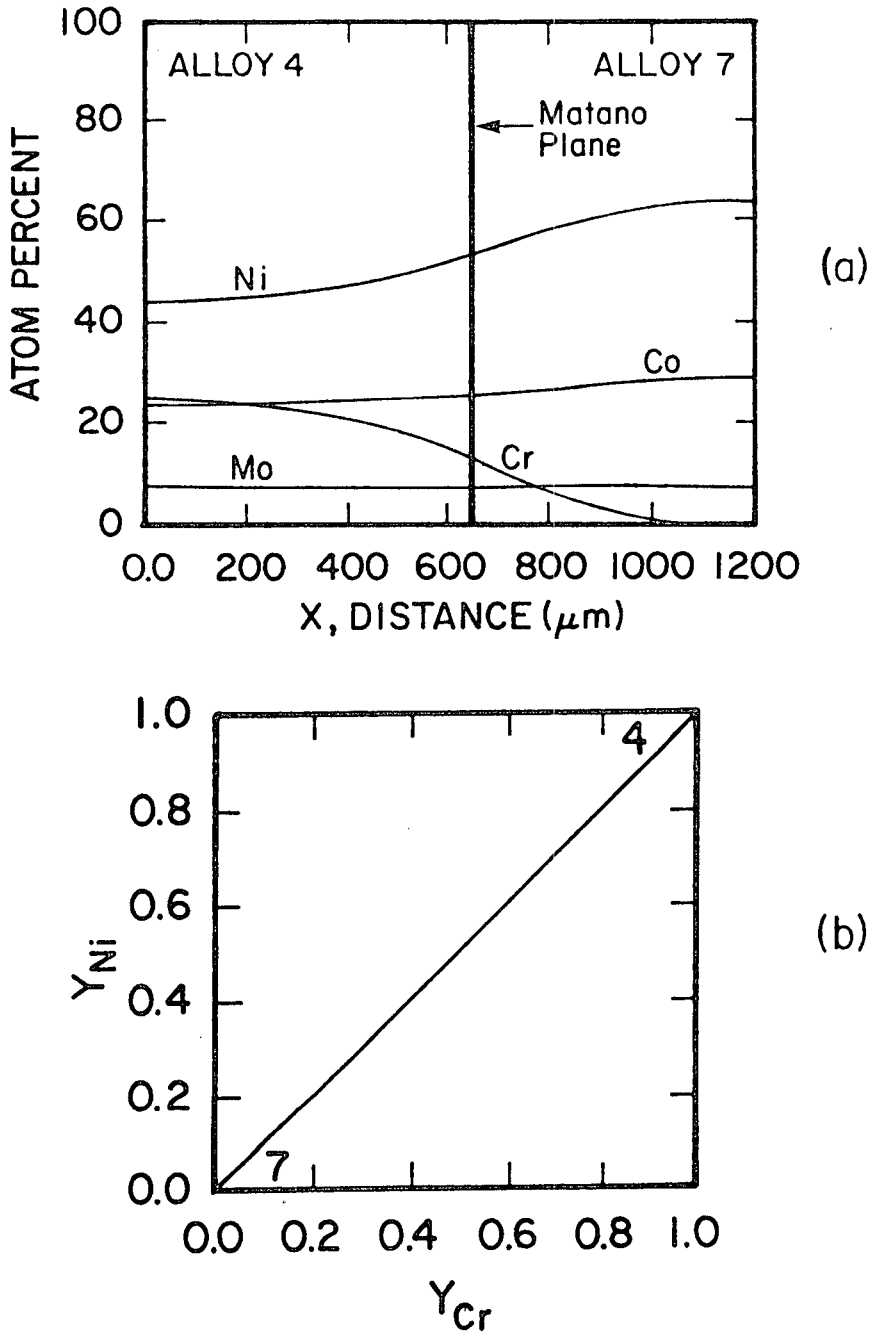


Fig. 4. (a) Concentration profiles and (b) the diffusion path for the couple 4/7.

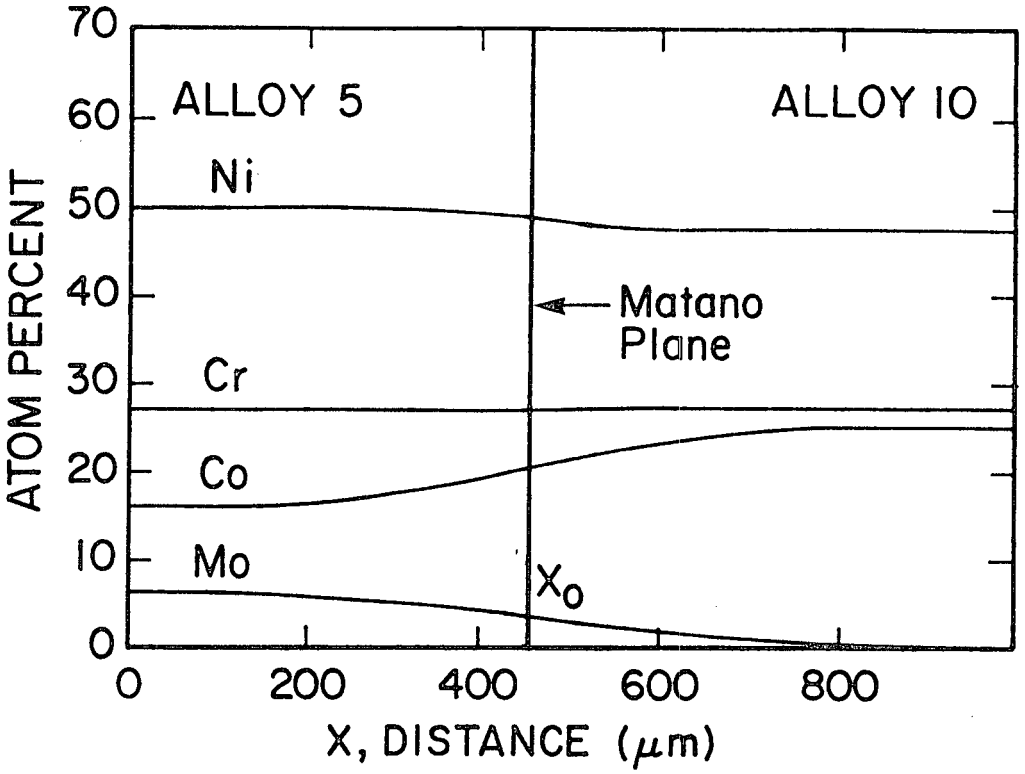


(a)

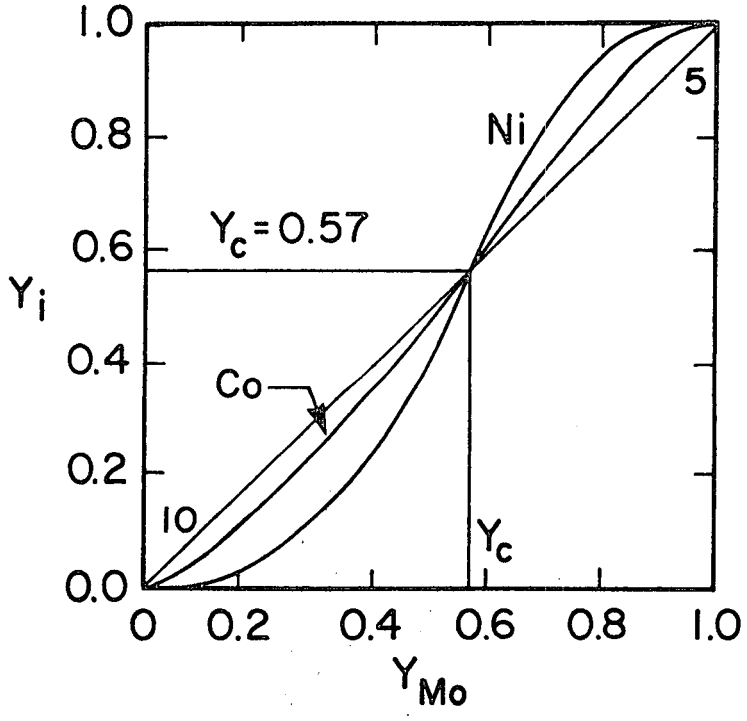


(b)

Fig. 5. (a) Concentration profiles and (b) the diffusion path representation for the couple 5/10.

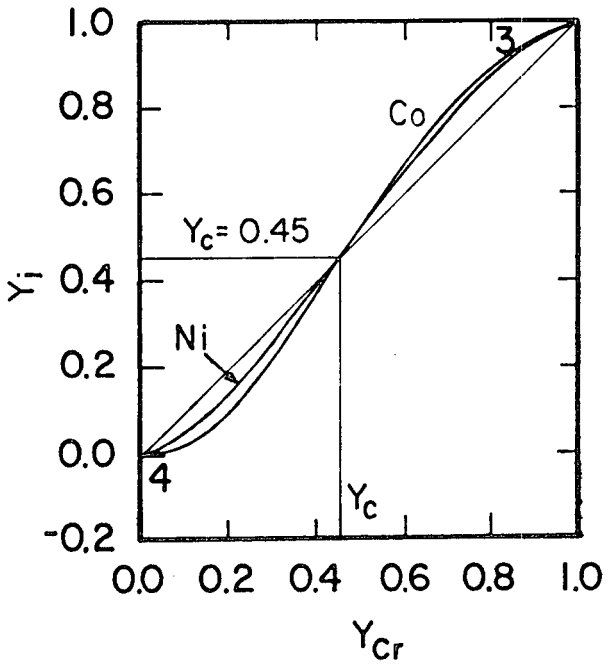


(a)

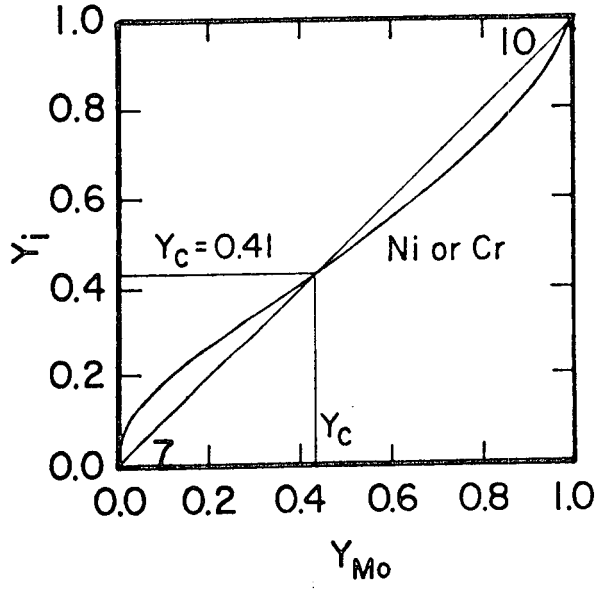


(b)

Fig. 6. Diffusion paths for (a) couple 3/4 and (b) couple 7/10.

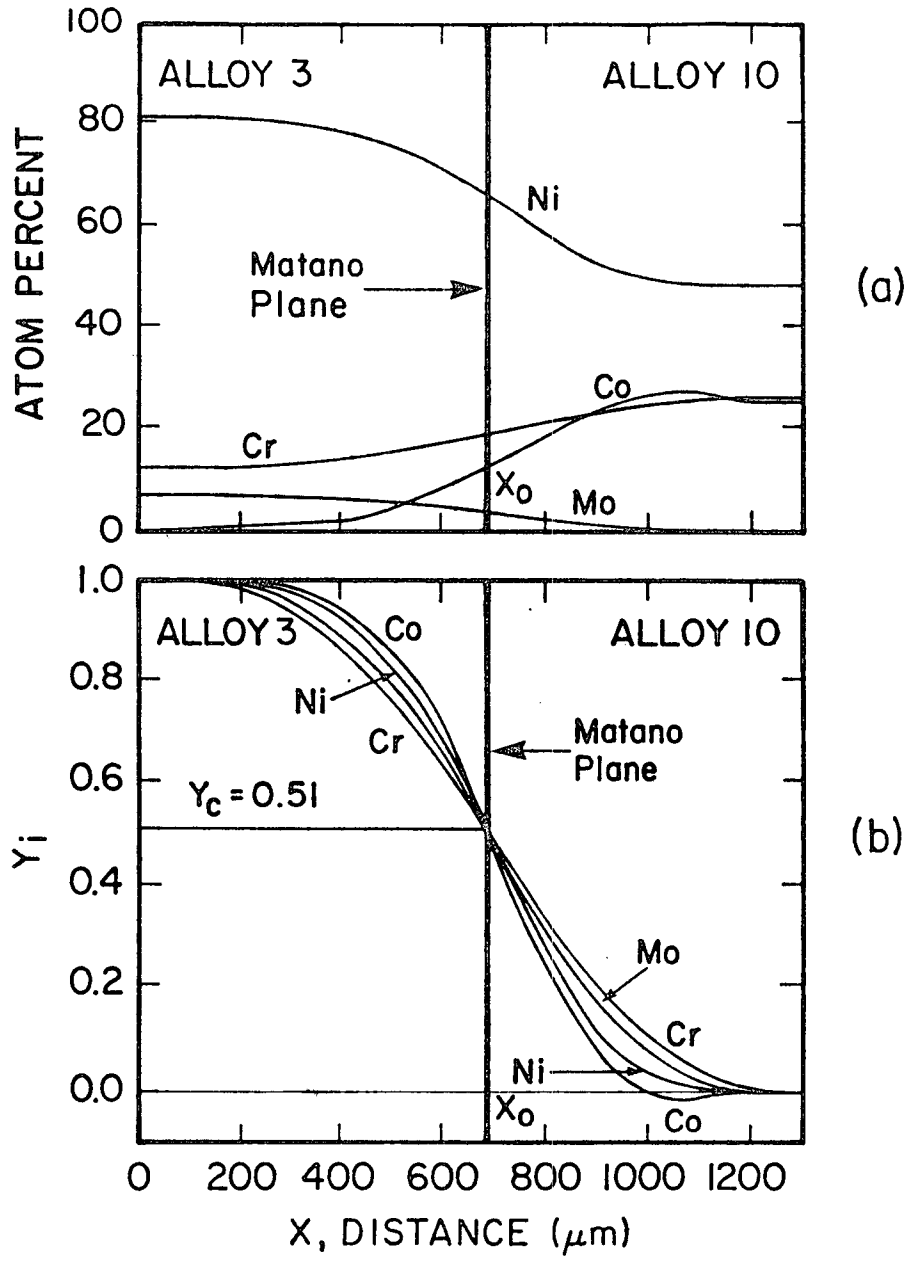


Fig. 7. Concentration profiles for the couple 3/10 with concentrations in (a) atom percent and (b) relative concentrations.

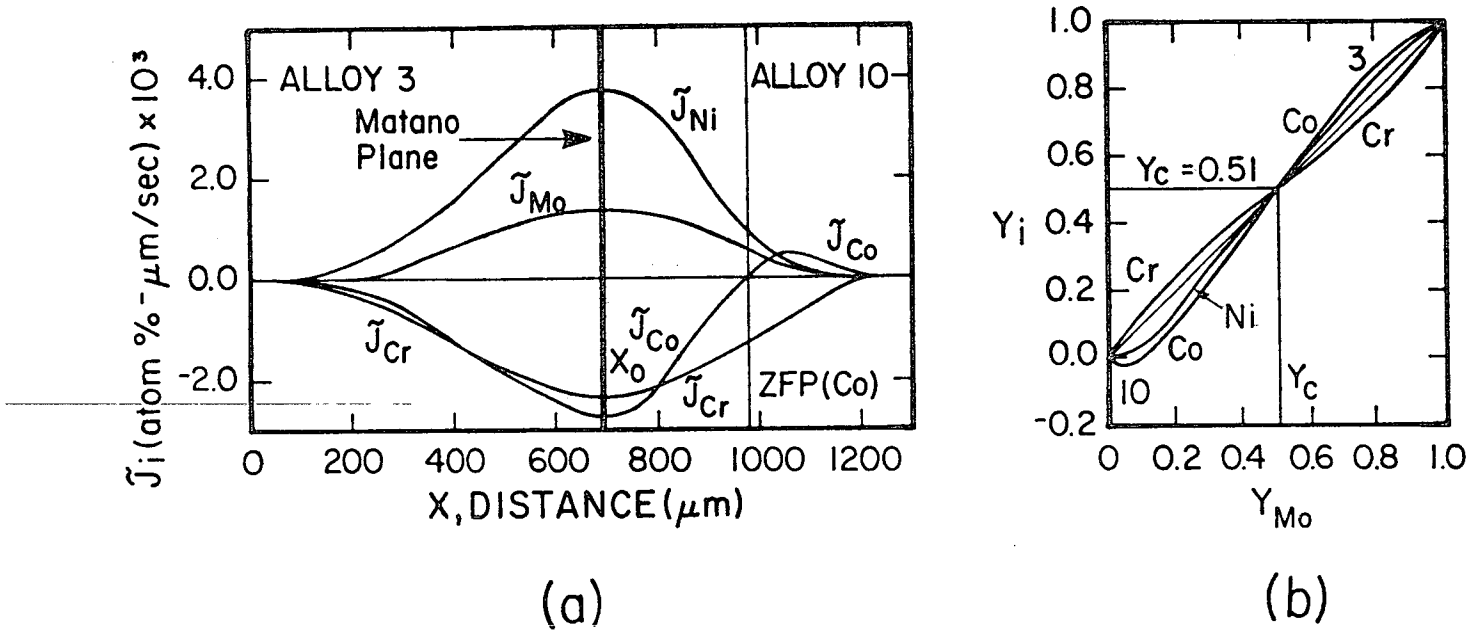


Fig. 8. (a) Profiles of interdiffusion fluxes and (b) the diffusion path representation for the couple 3/10.

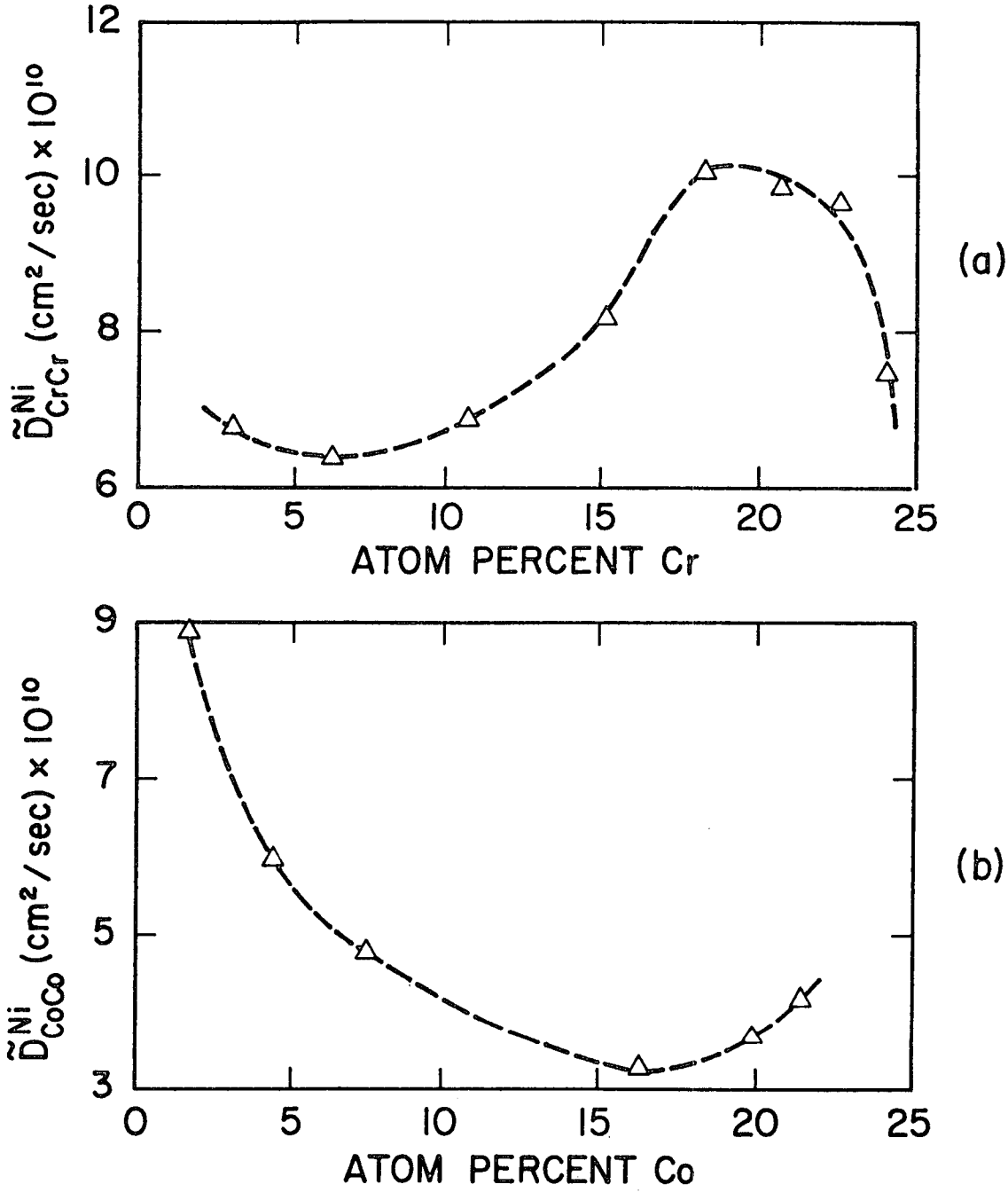


Fig. 9. Variation of quaternary interdiffusion coefficients (a) $\tilde{D}^{Ni}_{CrCr}$ and (b) $\tilde{D}^{Ni}_{CoCo}$ with composition, as calculated from the couples, 4/7 and 4/6, respectively.